Licorice Extracts Inhibits growth of Non-Small Cell Lung Cancer by Down-Regulating CDK4-Cyclin D1 Complex and Increasing CD8+ T Cell Infiltration

Ruifei Huang
North-West University https://orcid.org/0000-0001-8035-0307
Jinglin Zhu
North-West University
Ruijie Yang
North-West University
Yue Xiao
North-West University
Jiangna Yan
North-West University
Chunli Zheng
Northwest University
Wei Xiao
Jiangsu Kanion Pharmaceutical Co Ltd
Chao Huang (huangchao1989@nwafu.edu.cn)
Northwest University https://orcid.org/0000-0003-1186-0973
Yonghua Wang
North-West University

Primary research

Keywords: tumor microenvironment, NSCLC, licorice, systems pharmacology strategy

Posted Date: May 6th, 2021

DOI: https://doi.org/10.21203/rs.3.rs-488288/v1

Abstract

Background: Targeting tumor microenvironment (TME) may provide therapeutic activity and selectivity in treating cancers. Therefore, an improved understanding of the mechanism by which drug targeting TME would enable more informed and effective treatment measures. *Glycyrrhiza uralensis Fisch* (GUF, licorice), a widely used herb medicine, which has shown promising immunomodulatory activity and anti-tumor activity. However, the molecular mechanism of this biological activity has not been fully elaborated.

Methods: Here, potential active compounds and specific targets of licorice that trigger the antitumor immunity were predicted with a systems pharmacology strategy. Flow cytometry technique was used to detect cell cycle profile and $CD8^+$ T cell infiltration of licorice treatment. And anti-tumor activity of licorice was evaluated in C57BL/6 mice.

Results: We reported the G0/G1 growth phase cycle arrest of tumor cells induced by licorice that is related with the down-regulation of CDK4-Cyclin D1 complex, which subsequently led to increased protein abundance of PD-L1. Further, *in vivo* studies demonstrated that mitigation the outgrowth of NSCLC tumor induced by licorice was reliant on increased antigen presentation and improved $CD8^+$ T cell infiltration.

Conclusions: Briefly, our findings improved understanding of the anti-tumor effects of licorice with the systems pharmacology strategy, thereby promoting the development of natural products in the prevention or treatment of cancers.

Trial registration: Not applicable

Introduction

Lung cancer is the most prevalent diagnosed cancer worldwide and a major contributor of cancer mortality. And non-small cell lung cancer (NSCLC) accounts for approximately 85% of the diagnosed lung cancers[1–3]. In the recent years, immunotherapy targeting T cells has increasingly shown its potentiality in treatment of a wide variety of solid tumors, such as non-small cell lung cancer (NSCLC)[4–6]. Although encouraging, it is the fact that still only a small number of patients obtain long-term benefit, which is likely correlated with the complex network of the tumor microenvironment (TME)[7]. The tumor microenvironment (TME), a complex physical and biochemical system, playing a pivotal role in tumor initiation, progression, metastasis, and drug resistance[8]. It contains cells of the immune system, tumor cells, tumor vasculature and extracellular matrices (ECM)[9]. Among them, tumor cells could express inhibitory ligands that suppress the T-cell activity to evade immune destruction. Immune cells could produce some cytokines, growth factors, enzymes, and angiogenic mediators to promote growth of tumor[10]. And ECM consists of biological barriers around the tumor tissue to hamper lymphocyte penetration. Therefore, better understanding of the interactions in the TME that would increase the ratio of patients benefiting from these therapies are essential.

Traditional herb medicines and herbal derived components are playing increasingly critical roles in prevention and treatment of cancers[11, 12]. Compared with conventional chemotherapy, they are of low toxicity and pleiotropic actions, targeting the complex network of TME by modulating multiple cell-signaling pathways involved in immune. Thereby, natural products could be a great repository for development of novel therapeutic approaches in cancer treatment. As a well-known herbal medicine used worldwide for centuries, to date, several reports have been published complicating the immunomodulatory activity of licorice on multiple cancers, including colon cancer, breast cancer, acute myeloid leukemia, gastric cancer, melanoma, and prostate cancer[13–16]. However, the molecular underpinnings of this biological activity that licorice exert its immunomodulatory potential have not been fully elaborated.

To address this question, we used a systems pharmacology strategy to elaborate that how licorice exert anti-tumor effects by regulating multiple immune-related signaling pathways and targets, influencing cell cycle progression, and mitigate the growth of NSCLC cancer. First, by screening the poly-pharmacology molecules of licorice, predicting the targets of active compounds, constructing the networks, and linking the targets to the immune phenotype in lung cancer patients, we observed that active ingredients of licorice targeted a great variety of tumor-related signaling pathways, including cell cycle, inflammation, and migration. Then, we used *in vitro* and *in vivo* experiments to reveal anti-tumor effects of licorice. On the one hand, we found that licorice down-regulates CDK4-Cyclin D1 complex, resulting in G0/G1 phase arrest and increased PD-L1 levels in lung cancer cells. On the other hand, we also found that licorice increased antigen presentation and infiltration of $CD8^+$ T cell, significantly decreased tumor volume of mouse models of NSCLC *in vivo*. Taken together, our studies indicate that systems pharmacology strategy greatly uncovered the action mechanism of poly-pharmacology molecules of licorice, contributing the use of natural products for further anti-cancer drug development.

Results

1, Systems pharmacology uncovers that licorice targets cell cycle progression and immune process

As a comprehensive system, the systems pharmacology approach was used to investigate the complex molecular mechanisms of licorice as a treatment for NSCLC in this study (as shown in Fig. 1).

Altogether, 89 ingredients were identified in licorice with the searching literatures and using Traditional Chinese Medicine Systems Pharmacology Database (TCMSP), and a total of 23 active ingredients (shown in Table 1) were screened out by *in silico* ADME (absorption, distribution, metabolism, and excretion) system, with the criteria of oral bioavailability (OB) ≥ 50% and drug-likeness (DL) ≥ 0.40. Then, predicted by the weighted ensemble similarity method (WES) [17] and systematic drug targeting tool (SysDT)[18], we found that these 23 ingredients in licorice were investigated interacted with 109 targets (shown in Table 2 and table S1). And we constructed the compound-target (C-T) network graph to greatly illustrate the relationships between compounds and targets. In terms of the targets interacted with

licorice, we observed that most of which were related to cell cycle, immune, inflammation, cancer and neoplasm metastasis with higher scores. Specifically, including CDK2, ESR1, PPARG, ESRRA, PRKACA, CXCL8, PLAA, RXRB, MAPK14 and so on (shown in Fig. 2a).

To detect the potential role of these targets, we performed Gene Ontology (GO) biological processes enrichment analysis, and found that most of biological processes were involved in immune progress. Including “regulation of myeloid cell differentiation”, “neutrophil mediated immunity”, and “regulation of cytokine production involved in inflammatory response” (shown in Fig. 2b and 2c). Then, to further understand the relationship between licorice and diseases, using the Database for Annotation Visualization, and Integrated Discovery (DAVID), we performed the Kyoto Encyclopedia of Genes and Genomes (KEGG) pathway enrichment analysis. And the results showed that the most targets of licorice mainly enriched in signaling pathways related to the cancer process. Including “non-small cell lung cancer”, “small cell lung cancer” “pathways in cancer”, “prostate cancer”, “T cell receptor signaling pathway” and so on (Fig. 2d).

Therefore, the systems pharmacology analysis uncovers that licorice mainly targets cell cycle and immune progress to exert its anti-cancer effect, and paves the way for in-depth understanding of the multi-target molecular mechanism of licorice treating for NSCLC.

Table 1. Chemical information and pharmacokinetics parameters of 23 active compounds of licorice.

MOL-ID	Compounds	Structure	Categories	OB	DL	HL	Degree
MOL005008	Glycyrrhiza flavonol A	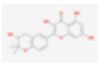	Flavonoids	41.28	0.60	13.71	30
MOL001484	Inermine	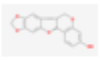	Flavonoids	75.18	0.54	11.72	35
MOL000211	Mairin	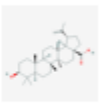	Saponins	55.38	0.78	8.87	16
MOL002311	Glycyrol	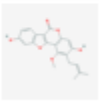	coumestans	90.78	0.67	9.85	14
MOL004808	glyasperin B	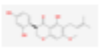	Others	65.22	0.44	16.1	31
MOL004810	glyasperin F	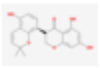	Others	75.84	0.54	15.64	33
MOL004820	kanzonols W	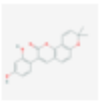	Flavonoids	50.48	0.52	0.15	38
MOL004855	Licoricone	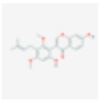	Flavonoids	63.58	0.47	16.37	23
MOL004863	3-(3,4-dihydroxyphenyl)-5,7-dihydroxy-8-(3-methylbut-2-enyl)chromon	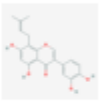	Others	66.37	0.41	15.81	26
MOL004879	Glycyrin	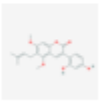	Coumarins	52.61	0.47	1.31	22
MOL004885	licoisoflavanone	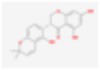	Flavonoids	52.47	0.54	15.67	31
MOL004891	shinpterocarpin	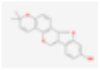	Flavonoids	80.3	0.73	6.5	44

MOL004903	liquiritin	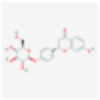	Flavonoids	65.69	0.74	17.96	21
MOL004904	licopyranocoumarin		Flavonoids	80.36	0.65	0.08	25
MOL004908	Glabridin	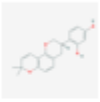	Flavonoids	53.25	0.47	0.03	39
MOL004912	Glabrone	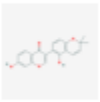	Flavonoids	52.51	0.5	16.09	38
MOL004914	1,3-dihydroxy-8,9-dimethoxy-6-benzofurano[3,2-c]chromenone	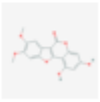	Others	62.9	0.53	9.32	20
MOL004959	1-Methoxyphaseollidin	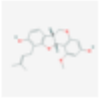	Flavonoids	69.98	0.64	9.53	35
MOL005001	Gancaonin H	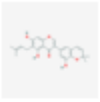	Others	50.1	0.78	16.64	30
MOL005003	Licoagrocarpin	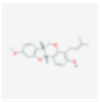	Flavonoids	58.81	0.58	9.45	37
MOL005007	Glyasperins M	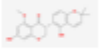	Flavonoids	72.67	0.59	15.57	39
MOL005012	Licoagroisoflavone	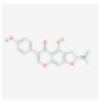	Flavonoids	57.28	0.49	19.64	36
MOL005017	Phaseol	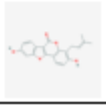	coumestans	78.77	0.58	9.64	21

OB, oral bioavailability; DL, drug-likeness; HL, Half-life

Table 2
The targets information of licorice.

UniProt-ID	Protein names	Gene names	Degree	Species
P0DP23	Calmodulin-1	CALM1	19	homo sapiens
P35368	Alpha-1B adrenergic receptor	ADRA1B	5	homo sapiens
P00918	Carbonic anhydrase 2	CA2	17	homo sapiens
P18031	Tyrosine-protein phosphatase non-receptor type 1	PTPN1	17	homo sapiens
P46098	5-hydroxytryptamine receptor 3A	HTR3A	1	homo sapiens
P20309	Muscarinic acetylcholine receptor M3	CHRM3	3	homo sapiens
P23219	Prostaglandin G/H synthase 1	PTGS1	8	homo sapiens
Q14524	Sodium channel protein type 5 subunit alpha	SCN5A	11	homo sapiens
P07477	Trypsin-1	PRSS1	18	homo sapiens
P17612	cAMP-dependent protein kinase catalytic subunit alpha	PRKACA	6	homo sapiens
O14757	Serine/threonine-protein kinase	CHEK1	18	homo sapiens
P11309	Serine/threonine-protein kinase pim-1	PIM1	20	homo sapiens
P35354	Prostaglandin G/H synthase 2	PTGS2	20	homo sapiens
P27487	Dipeptidyl peptidase 4	DPP4	13	homo sapiens
Q16539	Mitogen-activated protein kinase 14	MAPK14	13	homo sapiens
P48736	Phosphatidylinositol 4,5-bisphosphate 3-kinase catalytic subunit gamma isoform	PIK3CG	3	homo sapiens
P21730	C5a anaphylatoxin chemotactic receptor 1	AR	22	homo sapiens

UniProt-ID	Protein names	Gene names	Degree	Species
P49841	Glycogen synthase kinase-3 beta	GSK3B	17	homo sapiens
P24941	Cyclin-dependent kinase 2	CDK2	17	homo sapiens
Q92731	Estrogen receptor beta	ESR2	16	homo sapiens
P07900	Heat shock protein HSP 90-alpha	HSP90AA1	12	homo sapiens
P20248	Cyclin-A2	CCNA2	20	homo sapiens
B2RXH2	Lysine-specific demethylase 4E	KDM4E	1	homo sapiens
O00767	Stearoyl-CoA desaturase	SCD	10	homo sapiens
O95622	Adenylate cyclase type 5	ADCY5	7	homo sapiens
P08842	Steryl-sulfatase	STS	13	homo sapiens
P11474	Steroid hormone receptor ERR1	ESRRA	12	homo sapiens
P12644	Bone morphogenetic protein 4	BMP4	1	homo sapiens
P16152	Carbonyl reductase [NADPH] 1	CBR1	7	homo sapiens
P28223	5-hydroxytryptamine receptor 2A	HTR2A	18	homo sapiens
P51843	Nuclear receptor subfamily 0 group B member 1	NR0B1	7	homo sapiens
Q99814	Endothelial PAS domain-containing protein 1	EPAS1	3	homo sapiens
Q9Y263	Phospholipase A-2-activating protein	PLAA	3	homo sapiens
O60218	Aldo-keto reductase family 1 member B10	AKR1B10	1	homo sapiens
P05093	Steroid 17-alpha-hydroxylase/17,20 lyase	CYP17A1	1	homo sapiens

UniProt-ID	Protein names	Gene names	Degree	Species
P10276	Retinoic acid receptor alpha	RARA	1	homo sapiens
P11413	Glucose-6-phosphate 1-dehydrogenase	G6PD	1	homo sapiens
P11473	Vitamin D3 receptor	VDR	1	homo sapiens
P16662	UDP-glucuronosyltransferase 2B7	UGT2B7	1	homo sapiens
P18405	3-oxo-5-alpha-steroid 4-dehydrogenase 1	SRD5A1	1	homo sapiens
P19793	Retinoic acid receptor RXR-alpha	RXRA	7	homo sapiens
P36873	Serine/threonine-protein phosphatase PP1-gamma catalytic subunit	PPP1CC	1	homo sapiens
P80365	Corticosteroid 11-beta-dehydrogenase isozyme 2	HSD11B2	2	homo sapiens
Q08828	Adenylate cyclase type 1	ADCY1	1	homo sapiens
Q12908	Ileal sodium/bile acid cotransporter	SLC10A2	1	homo sapiens
Q9NRD8	Dual oxidase 2	DUOX2	1	homo sapiens
Q9UBM7	7-dehydrocholesterol reductase	DHCR7	1	homo sapiens
P03372	Estrogen receptor	ESR1	13	homo sapiens
P03420	Fusion glycoprotein F2	F2	18	homo sapiens
P37231	Peroxisome proliferator-activated receptor gamma	PPARG	19	homo sapiens
P30291	Wee1-like protein kinase	WEE1	3	homo sapiens
P23141	Liver carboxylesterase 1	CES2	7	homo sapiens
P05067	Amyloid-beta precursor protein	APP	7	homo sapiens

UniProt-ID	Protein names	Gene names	Degree	Species
P09960	Leukotriene A-4 hydrolase	LTA4H	10	homo sapiens
P10636	Microtubule-associated protein tau	MAPT	9	homo sapiens
Q04206	Transcription factor p65	RELA	6	homo sapiens
P22303	Acetylcholinesterase	ACHE	11	homo sapiens
Q15596	Nuclear receptor coactivator 2	NCOA2	10	homo sapiens
P11388	DNA topoisomerase 2-alpha	TOP2A	11	homo sapiens
P35968	Vascular endothelial growth factor receptor 2	KDR	8	homo sapiens
P00742	Coagulation factor X	F10	16	homo sapiens
P08709	Coagulation factor VII, EC 3.4.21.21	F7	7	homo sapiens
P11926	Ornithine decarboxylase	ODC1	10	homo sapiens
P14061	17-beta-hydroxysteroid dehydrogenase type 1	HSD17B1	5	homo sapiens
P18054	olyunsaturated fatty acid lipoxygenase ALOX12	ALOX12	7	homo sapiens
Q9UHC3	Acid-sensing ion channel 3	ASIC3	12	homo sapiens
P05091	Aldehyde dehydrogenase	ALDH2	4	homo sapiens
P37058	Testosterone 17-beta-dehydrogenase 3	HSD17B3	3	homo sapiens
Q13887	Krueppel-like factor 5	KLF5	2	homo sapiens
Q15788	Nuclear receptor coactivator 1	NCOA1	6	homo sapiens
Q12809	Potassium voltage-gated channel subfamily H member 2	KCNH2	5	homo sapiens

UniProt-ID	Protein names	Gene names	Degree	Species
Q9H4B7	Tubulin beta-1 chain	TUBB1	5	homo sapiens
P12268	Inosine-5'-monophosphate dehydrogenase 2	IMPDH2	1	homo sapiens
P11308	Transcriptional regulator ERG	ERG	1	homo sapiens
P45985	Dual specificity mitogen-activated protein kinase kinase 4	MAP2K4	1	homo sapiens
P25100	Alpha-1D adrenergic receptor	ADRA1D	2	homo sapiens
P36544	Neuronal acetylcholine receptor subunit alpha-7	CHRNA7	1	homo sapiens
P28702	Retinoic acid receptor RXR-beta	RXRB	2	homo sapiens
P08912	Muscarinic acetylcholine receptor M5	CHRM5	1	homo sapiens
P11229	Muscarinic acetylcholine receptor M1	CHRM1	2	homo sapiens
P07550	Beta-2 adrenergic receptor	ADRB2	4	homo sapiens
P35372	Mu-type opioid receptor	OPRM1	1	homo sapiens
P41143	Delta-type opioid receptor	OPRD1	1	homo sapiens
O60502	Protein O-GlcNAcase	OGA	1	homo sapiens
P08514	Integrin alpha-IIb	ITGA2B	1	homo sapiens
P16278	Beta-galactosidase	GLB1	1	homo sapiens
P28838	Cytosol aminopeptidase	LAP3	1	homo sapiens
P31639	Sodium/glucose cotransporter 2	SLC5A2	1	homo sapiens
P53396	ATP-citrate synthase	ACLY	1	homo sapiens

UniProt-ID	Protein names	Gene names	Degree	Species
P54577	Tyrosine–tRNA ligase, cytoplasmic	YARS	1	homo sapiens
O75907	Diacylglycerol O-acyltransferase 1	DGAT1	3	homo sapiens
P14222	Perforin-1	PRF1	1	homo sapiens
P51684	C-C chemokine receptor type 6	CCR6	2	homo sapiens
P05177	Cytochrome P450 1A2	CYP1A2	1	homo sapiens
Q16678	Cytochrome P450 1B1	CYP1B1	1	homo sapiens
Q92959	Solute carrier organic anion transporter family member 2A1	SLCO2A1	1	homo sapiens
P29474	Nitric oxide synthase	NOS3	2	homo sapiens
P08684	Cytochrome P450 3A4	CYP3A4	1	homo sapiens
P09211	Glutathione S-transferase P	GSTP1	2	homo sapiens
Q99835	Smoothened homolog	SMO	1	homo sapiens
Q9NYA1	Sphingosine kinase 1	SPHK1	1	homo sapiens
P48039	Melatonin receptor type 1A	MTNR1A	1	homo sapiens
Q03181	Peroxisome proliferator-activated receptor delta	PPARD	1	homo sapiens
P10145	Interleukin-8	CXCL8	1	homo sapiens
P62993	Growth factor receptor-bound protein 2	GRB2	1	homo sapiens
P01857	Immunoglobulin heavy constant gamma 1	IGHG1	2	homo sapiens
P35228	Nitric oxide synthase	NOS2	20	homo sapiens

UniProt-ID	Protein names	Gene names	Degree	Species
P04798	Cytochrome P450 1A1	CYP1A1	4	homo sapiens
Q12791	Calcium-activated potassium channel subunit alpha-1	KCNMA1	1	homo sapiens

2, Licorice induced tumor cells cycle arrest mainly by down-regulating Cyclin D1-CDK4

To further study the anti-cancer effect of licorice on NSCLC, we first tested the effects of licorice on the growth of tumor cells. According to the CCK8 assay results shown in Fig. 3a, we could recognize that licorice induced a concentration-dependent inhibition of H1975 cell proliferation. Treating licorice two days with concentrations of 3200, 5600 and 7200μg/mL, we found that compared with DMSO treatment, the H1975 cell growth decreased by 25, 48 and 87%, respectively. Moreover, the IC50 value on it were 5400μg/mL.

Next, given the analysis of systems pharmacology for licorice, and a number of studies have shown that the negative effects of licorice or its relatives on cell cycle progression[15, 16, 19, 20], we reasoned that licorice might influenced cell cycle to exert the anti-tumor effect on NSCLC to some extent. To test the hypothesis, we treated H1975 cells with different concentrations of licorice followed by flow cytometry analysis of cell cycle profile. Strikingly, H1975 cells subjected to licorice led to a significant increase in the number of cells arrested at G0/G1 growth phase, in a dose-dependent manner, compared with vehicle control containing media (shown in Fig. 3b and Fig. 3c). At the same time, the number of cells at both S growth phase and G2/M growth phase slightly decreased (Fig. 3c). This finding consistent with previous study that licorice induced G1 cell cycle arrest in MCF-7 human breast cancer cells[16].

It has been known that cyclin-dependent kinase (CDK)/cyclin complexes, such as CDK2/Cyclin E, CDK4, CDK6/CyclinD1, and P21 play crucial roles in cell cycle progression[21]. Therefore, to elucidate the underlying molecular mechanism with which licorice induced cell cycle arrest at G0/G1 growth phase, immunoblot analysis were performed to evaluate cell cycle-related protein abundance *in vitro* experiment. Notably, we found that the levels of CDK4, cyclin D1 were reduced, and the effect was concentration dependent, while the expression of CyclinB1 and CyclinA2 was relatively maintained at the level of the control group following licorice treatment (Fig. 3d and Fig. 3e). Interestingly, the expression of p21, a CDK inhibitor, was slightly decreased in response to licorice exposure vs control group (shown in Fig. 2d).

In addition, previous work uncovered that cyclin D1 degradation occurs mainly at the G1/S phase boundary[21, 22]. Collectively, these results indicated that licorice is likely to induce tumor cells arrested at G0/G1 growth phase by down-regulating CDK4-Cyclin D1 complex.

3, Licorice positively regulates PD-L1 protein abundance

It has been shown that PD-L1 expression can be modulated at both transcriptional and post-translational levels, however, it is not yet clear whether PD-L1 expression is regulated under physiological conditions for example during cell cycle progression[23–26]. In this setting, to further understand the connection between PD-L1 and cell cycle, we used cell synchronization by nocodazole arrest and immunoblot analysis to explore variation of PD-L1 during cell cycle. As shown in Fig. 4a and Fig. 4b, we found that PD-L1 protein expression increased in M/early G1 phases, followed by a great decrease in late G1/S phases.

As our results showed that licorice down-regulated Cyclin D1-CDK4 expression to arrest cell cycle progression, we probed whether licorice participated in variation of PD-L1. To do this, we treated H1975 cells with different concentration of licorice, followed by immunoblotting analysis. Strikingly, licorice administration results in a significant increase in the expression of PD-L1 protein (Fig. 4c and Fig. 4d), in a dose-dependent manner. Furthermore, recent finding had shown that Cyclin D-CDK4 kinase destabilized PD-L1, inhibition of CDK4/6 *in vivo* increased PD-L1 protein levels[27]. Together, these findings indicating that increased levels of PD-L1 expression by licorice correlated with down-regulation of Cyclin D1-CDK4 expression.

4、Licorice induce tumor regression by affecting Cyclin D1-CDK4-PD-L1 axis

Based on previous studies that various natural compounds in licorice possess effective antitumor activity[14, 16, 28, 29], we wanted to know whether licorice can function *in vivo* to suppress tumor progression for NSCLC. To do so, we utilized C57/BL6 female mice bearing LLC tumor to assess the anti-tumor impact of licorice. And size-matched tumor-bearing mice (TBMs) were divided into 4 groups randomly and received the administrations (as depicted in Fig. 5a).

By day 20 of treatment, as expected, all control mice encountered humane endpoints. Then mouse from each group were killed and dissected tumor, mouse serum was taken out and stored for subsequent experiment.

It is critical to note that licorice treatment result in a 64.9% tumor volume regression, and we found that there was slightly inhibitory effect on tumor volume of mice treated with anti-PD-L1 antibody alone vs control mice. Interestingly, we also observed a 54.7% tumor volume reduction in licorice + anti-PD-L1 mice compared with control mice over time. (Fig. 5a).

In keeping with our finding of tumor volume, treatment of licorice led to a significant induction of tumor weight, this also occurred in licorice + anti-PD-L1 group compared with untreated group. However, slight reduction of tumor weight was observed in anti-PD-L1 alone group (Fig. 5b).

Having pinpointed the critical role for licorice in affecting Cyclin D1-CDK4 expression *in vitro*, we next examined whether licorice had similar influence *in vivo*. Therefore, we assayed cell cycle-related protein for tumor tissue using the immunoblot method. Consistent with earlier observations *in vitro* (Fig. 3d),

licorice treatment markedly reduced the abundance of CDK4Cyclin D1, and importantly led to a dramatic PD-L1 accumulation compared with control group (Fig. 5c and 5d).

Therefore, these results coherently indicated that licorice might mainly function through down-regulating CDK4-Cyclin D1 to stabilize PD-L1 and subsequently suppress tumor progression.

5, Licorice increased antigen presentation and infiltration of $CD8^+$ T cell

Furthermore, the results of systems pharmacology analysis indicated that kinds of compounds of licorice correlated with $CD8^+$ T-cell (Fig. 6a, figure S2a, figure S2b), then intratumoral $CD8^+$ T-cell infiltration in tumor tissue lysates were measured by flow cytometry analysis. Importantly, $CD8^+$ T cell infiltration of licorice-treated mice we detected increased by 6% of that in untreated mice (Fig. 6c, Fig. 6d and figure S2c). In further support of a physiological role for licorice in promoting $CD8^+$T cell infiltration, we used the mice serum to perform ELISA-based assays and found a remarkable increase of IFN-γin licorice-treated mice (Fig. 6e). These results were in line with a previous study that CDK4/6 inhibitors induce breast cancer cell cytostasis and enhance their capacity to present antigen and stimulate cytotoxic T cells[30].

Next, to gain insights into the physiological role of licorice in modulating tumor regression at gene level, RT-qPCR analysis was performed. Specifically, we sought to determine relative mRNA levels of antigen presentation genes by RT-qPCR analysis, and observed that transporter–MHC interactions (Tap-bp) had at least a 15x fold increase in licorice-treated tumor tissues compared to control tumor samples, and peptide transporters (Tap1 and Tap2) were also markedly up-regulated in licorice-treated tumors, although directing peptide cleavage (Erap1) hardly change to some extent. (Fig. 6b).

Altogether, these studies indicated that licorice increased expression of antigen presentation genes and promoted $CD8^+$ T cell infiltration for tumor tissue.

Discussion

Natural products were shown broadly to interfere growth signals by multi-specific actions[31], which may open an opportunity to treat NSCLC effectively. In a panel of human cancers, licorice has been uncovered to provide growth-limiting activities[16, 28, 32]. Although changes in the cell-cycle have been noted under licorice treatment settings[19, 20], dissecting mechanism of the biological activity of licorice remains a challenge. Here, the critical findings of our study, summarized in Fig. 5c and Fig. 2d, include the discovery that licorice limits lung cancer growth mainly related with down-regulating CDK4-Cyclin D1 complex and enhancing intra-tumoral $CD8^+$ T cell infiltration. Our detailed investigation shows that licorice induce G1 cell-cycle arrest in lung cancer cells by inhibiting CDK4-Cyclin D1 complex, which in turn increase PD-L1 levels and antigen presentation and results in intra-tumoral $CD8^+$ T cell infiltration. These findings convincingly argue for a potential treatment option of licorice in the prevention and treatment of NSCLC.

Beginning with systems pharmacology analysis, flow cytometry analysis of cell cycle profile and immunoblotting, we observed that licorice treatment led to G1 cell-cycle arrest and inhibit the expression of CDK4-Cyclin D1 complex in H1975 cells. This biological activity was further validated in licorice-treated tumor. It is well known that CDK4-Cyclin D1 complex were required for progression of cells cycle through the G0/G1 phase[33–35], which would suggest that G1 cell-cycle arrest is largely associated with decreased levels of CDK4-Cyclin D1 after licorice treatment. One of the strongest links between CDK4-Cyclin D1 complex down-regulation and tumor regression has come from inhibitor studies. As a kind of CDK4/6 inhibitors, abemaciclib caused regression of bulky tumors in mouse models of mammary carcinoma[30]. Furthermore, many human cancers harbor genomic or transcriptional aberrations that could activate CDK4/6[36–38]. Therefore, our finding that licorice inhibit the expression of CDK4-Cyclin D1 complex would be critically important for prevention and treatment of cancers.

Moreover, Cyclin D/CDK4 was found negatively regulates PD-L1 protein stability in several tumor cell lines[27, 39]. And previous studies revealed that response to PD-1/PD-L1 blockade might correlate with PD-L1 expression levels in tumor cells[40–42]. Notably, we discovered that licorice treatment induced increased expression of PD-L1 levels both *in vitro* and *in vivo*. These studies, together with our findings, shed light on a viable option for the management of NSCLC, with or without other treatments in conjunction, to enhance the efficiency of cancer immunotherapies.

The functional impairment of T cell-mediated immunity in the TME is a defining feature sharing by many cancers, and $CD8^+$ T cells became the central focus of new cancer therapeutics[43, 44]. Due to the data that shows licorice increased expression of antigen presentation genes and promoted $CD8^+$ T cell infiltration for tumor tissue, we reasoned that $CD8^+$ T cell infiltration contribute to growth inhibition for tumor.

In summary, this study evidenced that licorice induced G0/G1 phase cell cycle arrest by down-regulating CDK4-Cyclin D1 complex on tumor cells, in addition, licorice increased expression of antigen presentation genes and infiltration of CD8 + T cell in tumor microenvironment. Therefore, this study illuminated a novel mechanism of anti-tumor effect of licorice in NSCLC treatment, and provide functional evidence for development of natural products in anti-tumor immunity.

Methods

Pharmacokinetic evaluation

the ingredients of licorice were identified based on searching literatures and using Traditional Chinese Medicine Systems Pharmacology Database (TCMSP, http://tcmspw.com/)[45] and active ingredients (shown in Table 1) were further screened out by in silico ADME system, with the criteria of oral bioavailability (OB) ≥ 50% and drug-likeness (DL) ≥ 0.40.

Target fishing and validation

We identified direct targets of licorice on the basis of a WES method and a SysDT tool, then obtained targets were uploaded to Uniprot (http://www.uniprot.org)[46] to normalize their name and organisms. And the targets of Homo sapiens were chosen for further investigation. We used Cytoscape 3.7.0 software to construct and analyze compound-target network.

GO enrichment analysis and KEGG analysis for targets.

(GO) enrichment analysis and KEGG analysis was performed through mapping targets to DAVID (http://david.abcc.ncifcrf.gov) for classification. We chose the terms with P value less than 0.05.

Cell proliferation assay

Cellular proliferation was assayed using a Cell Counting Kit-8 (CCK-8, Beyotime, China). In brief, 1×10^4 cells were seeded in 96-well microplates. After 24 h, cells were treated with different concentrations of licorice or vehicle for 48 h. Then, 10 μ L CCK-8 solution was added to each well and incubated at 37°C for 4 h. Absorbance at 450 nm was measured using a microplate reader (Molecular Devices, California, USA)

Cell lines, compounds, and reagents

H1975LLC (Shanghai, China) were maintained in RPMI medium (C11875500BT,Gibco, Thermo Fisher Scientific) or DMEM (C11995500BT, Gibco, Thermo Fisher Scientific) supplemented with 10% fetal bovine serum (10099141, Gibco, Thermo Fisher Scientific).

Licorice powder was purchased from LEMETIAN MEDICINE. And Typical HPLC chromatogram of licorice extract performed by LEMETIAN MEDICINE (figure S1).

FACS analysis of cell cycle

Once H1975 cells achieved a 70–80% confluency, they were treated with 0.1% DMSO or different concentration of licorice for 48 h. Then, cells were fixed with ice-cold 70% ethanol at -20°C overnight. After fixation, cells were washed thrice with cold PBS and then stained with Cell Cycle and Apoptosis Analysis Kit (C1052, Beyotime Biotechnology) according to the manufacturer's instructions. Samples were then analyzed using a NovoCyte Flow Cytometer (ACEA Biosciences). The results were analyzed by Flow Jo software (BD bioscience.

Western blotting

For western blot analysis, cells or tumor tissue were lysed in lysis buffer from the Qproteome Mammalian Protein Prep Kit (37901, QIAGEN) with the addition of protease inhibitors after PBS washing. Protein concentrations were measured by a microplate reader (Molecular Devices, California, USA) using the BCA Protein Assay Kit (Beyotime, China). Then equal amounts of protein were resolved on SDS-PAGE and transferred to nitrocellulose membranes ((Millipore, Bedford, MA, USA)) and incubated with primary antibodies against: mouse monoclonal CDK4, cyclin D1 (BD Bioscience, USA); cyclin A2, cyclin B1, P21, PD-L1, B-actin, GAPDH (Santa Cruz Biotechnology, USA) and β-actin (abcam); Secondary antibodies were goat anti-rabbit HRP. Immunoreactive polypeptides were detected by electrochemiluminescence (ECL)

reagents (Cat#170–5061, Bio Rad) using ChemiDoc™ XRS + Imaging System (Bio-Rad). Western blot band intensity quantification was calculated using ImageJ.

Cell synchronization and FACS analyses

For synchronization into the G2/M phase of the cell cycle progression, H1975 cells were treated with 100 ng/mL of nocodazole (M1404, Sigma-Aldrich) for 16 hours. Then cells release was collected at the indicated time points and fixed by 70% ethanol at − 20°C overnight. After fixation, cells were washed 3 times with cold PBS and stained with Cell Cycle and Apoptosis Analysis Kit (C1052, Beyotime Biotechnology) according to the manufacturer's instructions. Stained cells were sorted with NovoCyte Flow Cytometer (ACEA Biosciences). The results were analyzed by Flow Jo software (BD bioscience).

Experimental Model in vivo and Subject Details

All animal protocols described in this study were approved by the Institutional Animal Care and Use Committee (IACUC: 2018120202) at The Kanion Parmaceutical. C57BL/6 female mice (purchased from The Comparative medicine center of Yangzhou University) with 6–8 weeks of age were used. To generate tumor model, $5*10^5$ LLC cells were injected into the flanks of mice. Two days after inoculation, mice were randomized into four groups and treated with licorice, licorice + PD-L1, PD-L1 or vehicle for 2 weeks. Licorice was administered daily by gastric gavage (200 mg/kg of body weight); Anti-PD-L1 (B7-H1) (10F.9G2) (BE0101, BioXCell) was administered by intraperitoneal (i.p.) injection on day 4, 7, and 10 after inoculation. (200 mg/kg of body weight); control mice were treated with vehicle (0.9% NaCL) 5 ml/kg by intraperitoneal (i.p.) injection. Tumor size was measured as indicated in the figures, and tumor volume was calculated by using the formula: 1/2×length× $width^2$. Mice with tumors greater than 1,500 mm^3 were sacrificed and tumors were collected and snap-frozen.

Real-Time RT-PCR analyses

Total RNAs were extracted using the RNeasy mini kit (74106, QIAGEN), and reverse transcription reactions were performed using the Prime Script RT reagent Kit with gDNA Eraser (Perfect Real Time) (RR047A, Takara). After mixing the generated cDNA templates with primers/probes and Green® Premix Ex Taq™ II (Tli RNaseH Plus) (RR820B (A × 2), Takara), reactions were performed with the Step One Plus TM Real-Time PCR System (Applied Biosystems).

Mouse GAPDH: Forward, 5'-AGGTCGGTGTGAACGGATTTG-3',

Reverse, 5'-GGGGTCGTTGATGGCAACA-3';

Mouse Tap1: Forward, GGACTTGCCTTGTTCCGAGAG,

Reverse, GCTGCCACATAACTGATAGCGA;

Mouse Tap-2: Forward, CTGGCGGACATGGCTTTACTT,

Reverse, CTCCCACTTTTAGCAGTCCCC;

Mouse Tap-bp: Forward, GGCCTGTCTAAGAAACCTGCC

Reverse, CCACCTTGAAGTATAGCTTTGGG

Mouse Erap1: Forward, TAATGGAGACTCATTCCCTTGGA

Reverse, AAAGTCAGAGTGCTGAGGTTTG

Single cell generation from tumor tissue and flow cytometry analysis

Tumor tissues were minced and digested with Collagenase IV (2mg/ml, 17104-019, Gibco) and DNase I (2000U/ml, D7073, Beyotime) and Hyaluronidase (0.5mg/ml, S10060, YuanYe Biotechnology) and Dispase Ⅱ (0.5mg/ml, S25046, YuanYe Biotechnology) in DMEM for 30 min at 37°C. Cells were then collected by centrifuge and filtered through a 70 μ m strainer (15-1070 BIOLOGIX) in DMEM. Cell pellets were suspended and lysed in red blood cell lysis buffer (Beyotime Biotechnology) for 5 min. The cells were then filtered through a 40 μ m strainer (15-1040, BIOLOGIX) in 1 x PBS with 2% BSA. $1*10^6$ cells were incubated with antibodies against Anti-mouse CD3e APC (145-2C11) (05122-80-25, Biogems), Anti-mouse CD8a PE (53 − 6.7) (100707, BioLegend), Anti-mouse CD45 PE/Cy7 (30-F11) (103114, BioLegend) at room temperature for 30 min. Cells were washed by 1 x PBS with 2% BSA 3 times and detected by NovoCyte Flow Cytometer (ACEA Biosciences).

Elisa analysis

Cytokines of mouse serum in licorice-treated group and control group were analyzed according to the manufacturer's recommendations: Mouse IFN-γ Immunoassay (USA R&D Systems, Inc.). Absorbance was measured on a microplate reader (Molecular Devices, California, USA) using Prism 8.0.2 (GraphPad Software, Inc.).

QUANTIFICATION AND STATISTICAL ANALYSIS

Statistical analyses were performed with Prism 8.0.2 (GraphPad Software, Inc.). Two groups comparison using student's t test. Multiple comparisons using one-way analysis of variance (ANOVA) followed by Tukey test. Tumor volume were analyzed using two-way ANOVA followed by Tukey test. Differences were considered statistically significant at a p value ≤ 0.05. Data are presented as the mean ± SEM. * $p < 0.05$, ** $p < 0.01$, *** $p < 0.001$, **** $p < 0.0001$. All data shown is representative two or more independent experiments, unless indicated otherwise.

Declarations

Declarations

Ethics approval and consent to participate

All animal protocols described in this study were approved by the Institutional Animal Care and Use Committee (IACUC: 2018120202) at The Kanion Parmaceutical.

Consent for publication

We would like to declare on behalf of my co-authors that the work described was original research that has not been published previously, and not under consideration for publication elsewhere, in whole or in part. No conflict of interest exits in the submission of this manuscript, and manuscript is approved by all authors for publication.

Availability of data and materials

All other data are included within the Article or Supplementary Information or available from the authors on request.

Competing interests

The authors declare no competing interests.

Funding

This work was supported by the National Natural Science Foundation of China (Grant No. 81803960), the 64th batch of postdoctoral general programs in China (Grant No. 2018M643723), and National Science and Technology Major Project of China (Grant No. 2019ZX09201004-001).

Authors' contributions

Ruifei Huang and Jinglin Zhu contributing equally to this work. Ruifei Huang, Jinglin Zhu, Ruijie Yang, and Yue Xiao, Jiangna Yan carried out the experiment. Ruifei Huang wrote the manuscript with support from Chunli Zheng and Chao Huang. Wei Xiao and Yonghua Wang helped supervise the project. Chunli Zheng and Chao Huang conceived the original idea.

Acknowledgements

We thank Jiangsu Kanion Pharmaceutical, Co., ltd. for helpful experimental support.

References

1. Ferlay, J., et al., *Estimating the global cancer incidence and mortality in 2018: GLOBOCAN sources and methods.* Int J Cancer, 2019. **144**(8): p. 1941-1953.
2. Kao, S., et al., *IGDB.NSCLC: integrated genomic database of non-small cell lung cancer.* Nucleic Acids Res, 2012. **40**(Database issue): p. D972-7.
3. Al-Yozbaki, M., et al., *Targeting DNA methyltransferases in Non-small-cell lung cancer.* Semin Cancer Biol, 2021.
4. Pilipow, K., A. Darwich, and A. Losurdo, *T-cell-based breast cancer immunotherapy.* Semin Cancer Biol, 2020.

5. Zheng, H., et al., *HDAC Inhibitors Enhance T-Cell Chemokine Expression and Augment Response to PD-1 Immunotherapy in Lung Adenocarcinoma.* Clin Cancer Res, 2016. **22**(16): p. 4119-32.
6. Edwards, J., et al., *CD103(+) Tumor-Resident CD8(+) T Cells Are Associated with Improved Survival in Immunotherapy-Naive Melanoma Patients and Expand Significantly During Anti-PD-1 Treatment.* Clin Cancer Res, 2018. **24**(13): p. 3036-3045.
7. Chabanon, R.M., et al., *PARP inhibition enhances tumor cell-intrinsic immunity in ERCC1-deficient non-small cell lung cancer.* J Clin Invest, 2019. **129**(3): p. 1211-1228.
8. Zhou, Z. and Z.-R. Lu, *Molecular imaging of the tumor microenvironment.* Advanced Drug Delivery Reviews, 2017. **113**: p. 24-48.
9. Tang, H., J. Qiao, and Y.-X. Fu, *Immunotherapy and tumor microenvironment.* Cancer Letters, 2016. **370**(1): p. 85-90.
10. Becht, E., A. de Reyniès, and W.H. Fridman, *Integrating tumor microenvironment with cancer molecular classifications.* Genome Medicine, 2015. **7**(1).
11. Xu, J., et al., *Synergistic Effect and Molecular Mechanisms of Traditional Chinese Medicine on Regulating Tumor Microenvironment and Cancer Cells.* Biomed Res Int, 2016. **2016**: p. 1490738.
12. He, J., P. Yin, and K. Xu, *Effect and Molecular Mechanisms of Traditional Chinese Medicine on Tumor Targeting Tumor-Associated Macrophages.* Drug Des Devel Ther, 2020. **14**: p. 907-919.
13. Niu, Y., J. Xu, and T. Sun, *Cyclin-Dependent Kinases 4/6 Inhibitors in Breast Cancer: Current Status, Resistance, and Combination Strategies.* J Cancer, 2019. **10**(22): p. 5504-5517.
14. Kanazawa, M., et al., *Isoliquiritigenin Inhibits the Growth of Prostate Cancer.* European Urology, 2003. **43**(5): p. 580-586.
15. Hsu, Y.L., P.L. Kuo, and C.C. Lin, *Isoliquiritigenin induces apoptosis and cell cycle arrest through p53-dependent pathway in Hep G2 cells.* Life Sci, 2005. **77**(3): p. 279-92.
16. Jo, E.H., et al., *Chemopreventive properties of the ethanol extract of chinese licorice (Glycyrrhiza uralensis) root: induction of apoptosis and G1 cell cycle arrest in MCF-7 human breast cancer cells.* Cancer Lett, 2005. **230**(2): p. 239-47.
17. Zheng, C., et al., *Large-scale Direct Targeting for Drug Repositioning and Discovery.* Sci Rep, 2015. **5**: p. 11970.
18. Yu, H., et al., *A systematic prediction of multiple drug-target interactions from chemical, genomic, and pharmacological data.* PLoS One, 2012. **7**(5): p. e37608.
19. Zhou, Y. and W.S. Ho, *Combination of liquiritin, isoliquiritin and isoliquirigenin induce apoptotic cell death through upregulating p53 and p21 in the A549 non-small cell lung cancer cells.* Oncol Rep, 2014. **31**(1): p. 298-304.
20. Ii, T., et al., *Induction of cell cycle arrest and p21(CIP1/WAF1) expression in human lung cancer cells by isoliquiritigenin.* Cancer Lett, 2004. **207**(1): p. 27-35.
21. Alao, J.P., *The regulation of cyclin D1 degradation: roles in cancer development and the potential for therapeutic invention.* Mol Cancer, 2007. **6**: p. 24.

22. M Hitomi , D.W.S., *Cyclin D1 production in cycling cells depends on ras in a cell-cycle-specific manner.* Curr Biol, 1999. **9**(19): p. 1075-84.
23. Casey, S.C., et al., *MYC regulates the antitumor immune response through CD47 and PD-L1.* Science, 2016. **352**(6282): p. 227-31.
24. Dorand, R.D., et al., *Cdk5 disruption attenuates tumor PD-L1 expression and promotes antitumor immunity.* Science, 2016. **353**(6297): p. 399-403.
25. Li, C.W., et al., *Glycosylation and stabilization of programmed death ligand-1 suppresses T-cell activity.* Nat Commun, 2016. **7**: p. 12632.
26. Lim, S.O., et al., *Deubiquitination and Stabilization of PD-L1 by CSN5.* Cancer Cell, 2016. **30**(6): p. 925-939.
27. Zhang, J., et al., *Cyclin D-CDK4 kinase destabilizes PD-L1 via cullin 3-SPOP to control cancer immune surveillance.* Nature, 2018. **553**(7686): p. 91-95.
28. Hong, S.H., et al., *Anti-Proliferative and Pro-Apoptotic Effects of Licochalcone A through ROS-Mediated Cell Cycle Arrest and Apoptosis in Human Bladder Cancer Cells.* Int J Mol Sci, 2019. **20**(15).
29. Ayeka, P.A., et al., *The immunomodulatory activities of licorice polysaccharides (Glycyrrhiza uralensis Fisch.) in CT 26 tumor-bearing mice.* BMC Complement Altern Med, 2017. **17**(1): p. 536.
30. Goel, S., et al., *CDK4/6 inhibition triggers anti-tumour immunity.* Nature, 2017. **548**(7668): p. 471-475.
31. Chen, X., et al., *Celastrol induces ROS-mediated apoptosis via directly targeting peroxiredoxin-2 in gastric cancer cells.* Theranostics, 2020. **10**(22): p. 10290-10308.
32. Wu, X., et al., *Glycyrrhizin Suppresses the Growth of Human NSCLC Cell Line HCC827 by Downregulating HMGB1 Level.* Biomed Res Int, 2018. **2018**: p. 6916797.
33. Y Dong , L.S., K Sugimoto, Y Tai, M Tokuda, *Cyclin D1-CDK4 complex, a possible critical factor for cell proliferation and prognosis in laryngeal squamous cell carcinomas.* Int J Cancer, 2001. **95**(4): p. 209-15.
34. Schade, A.E., et al., *Cyclin D-CDK4 relieves cooperative repression of proliferation and cell cycle gene expression by DREAM and RB.* Oncogene, 2019. **38**(25): p. 4962-4976.
35. Topacio, B.R., et al., *Cyclin D-Cdk4,6 Drives Cell-Cycle Progression via the Retinoblastoma Protein's C-Terminal Helix.* Mol Cell, 2019. **74**(4): p. 758-770 e4.
36. Hamilton, E. and J.R. Infante, *Targeting CDK4/6 in patients with cancer.* Cancer Treat Rev, 2016. **45**: p. 129-38.
37. K Lingfei , Y.P., L Zhengguo, G Jianhua, Z Yaowu, *A study on p16, pRb, cdk4 and cyclinD1 expression in non-small cell lung cancers.* Cancer Lett, 1998. **130**(1-2): p. 93-101.
38. H-B Sun , X.-L.H., M Zhong, D-J Yu, *Linc00703 suppresses non-small cell lung cancer progression by modulating CyclinD1/CDK4 expression.* Eur Rev Med Pharmacol 2020. **24**(11): p. 6131-6138.
39. Jin, X., et al., *Phosphorylated RB Promotes Cancer Immunity by Inhibiting NF-kappaB Activation and PD-L1 Expression.* Mol Cell, 2019. **73**(1): p. 22-35 e6.

40. Chen, L., et al., *CD38-Mediated Immunosuppression as a Mechanism of Tumor Cell Escape from PD-1/PD-L1 Blockade.* Cancer Discov, 2018. **8**(9): p. 1156-1175.
41. Herbst, R.S., et al., *Predictive correlates of response to the anti-PD-L1 antibody MPDL3280A in cancer patients.* Nature, 2014. **515**(7528): p. 563-7.
42. Iwai, Y., *Involvement of PD-L1 on tumor size in the escape from host immune systerm and tumor immunotherapy by PD-L1 blocked.* Proc Natl Acad Sci U S A **99**(19): p. 12293-7.
43. Maimela, N.R., S. Liu, and Y. Zhang, *Fates of CD8+ T cells in Tumor Microenvironment.* Comput Struct Biotechnol J, 2019. **17**: p. 1-13.
44. Lanitis, E., et al., *Mechanisms regulating T-cell infiltration and activity in solid tumors.* Ann Oncol, 2017. **28**(suppl_12): p. xii18-xii32.
45. Ru, J., et al., *TCMSP: a database of systems pharmacology for drug discovery from herbal medicines.* J Cheminform, 2014. **6**: p. 13.
46. UniProt, C., *UniProt: a worldwide hub of protein knowledge.* Nucleic Acids Res, 2019. **47**(D1): p. D506-D515.

Figures

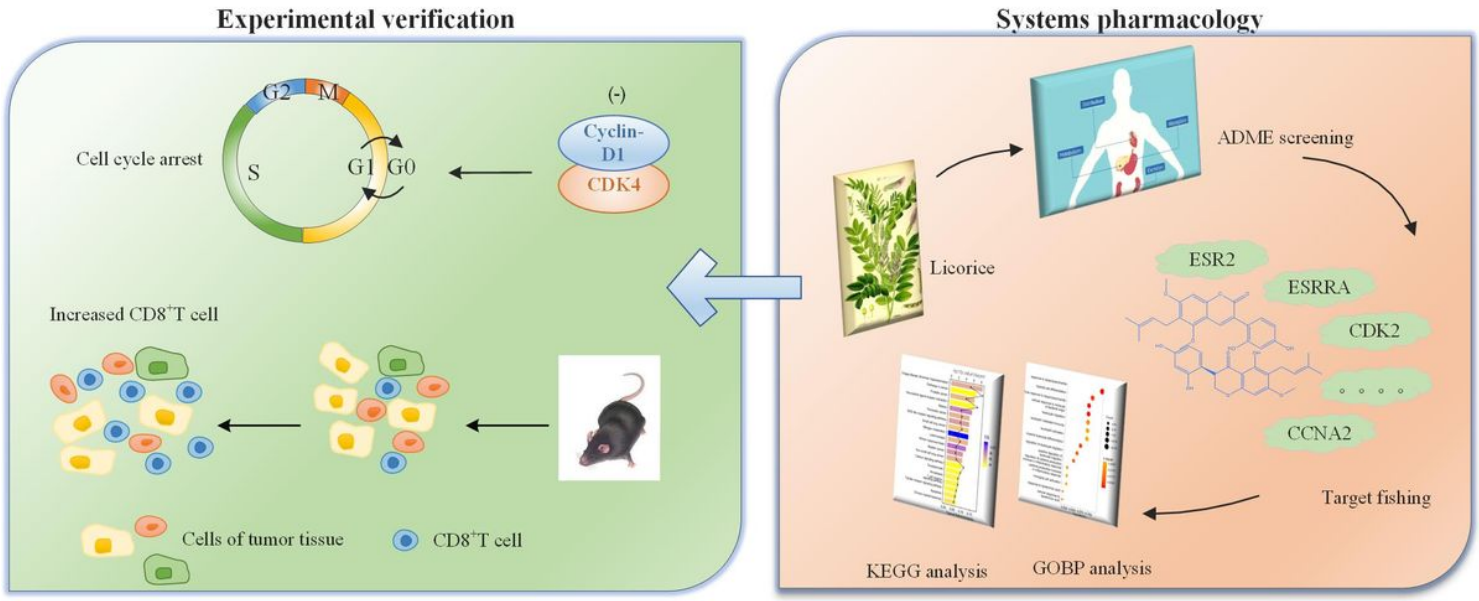

Figure 1

Workflow of systems pharmacology analysis to undercover mechanism of licorice.

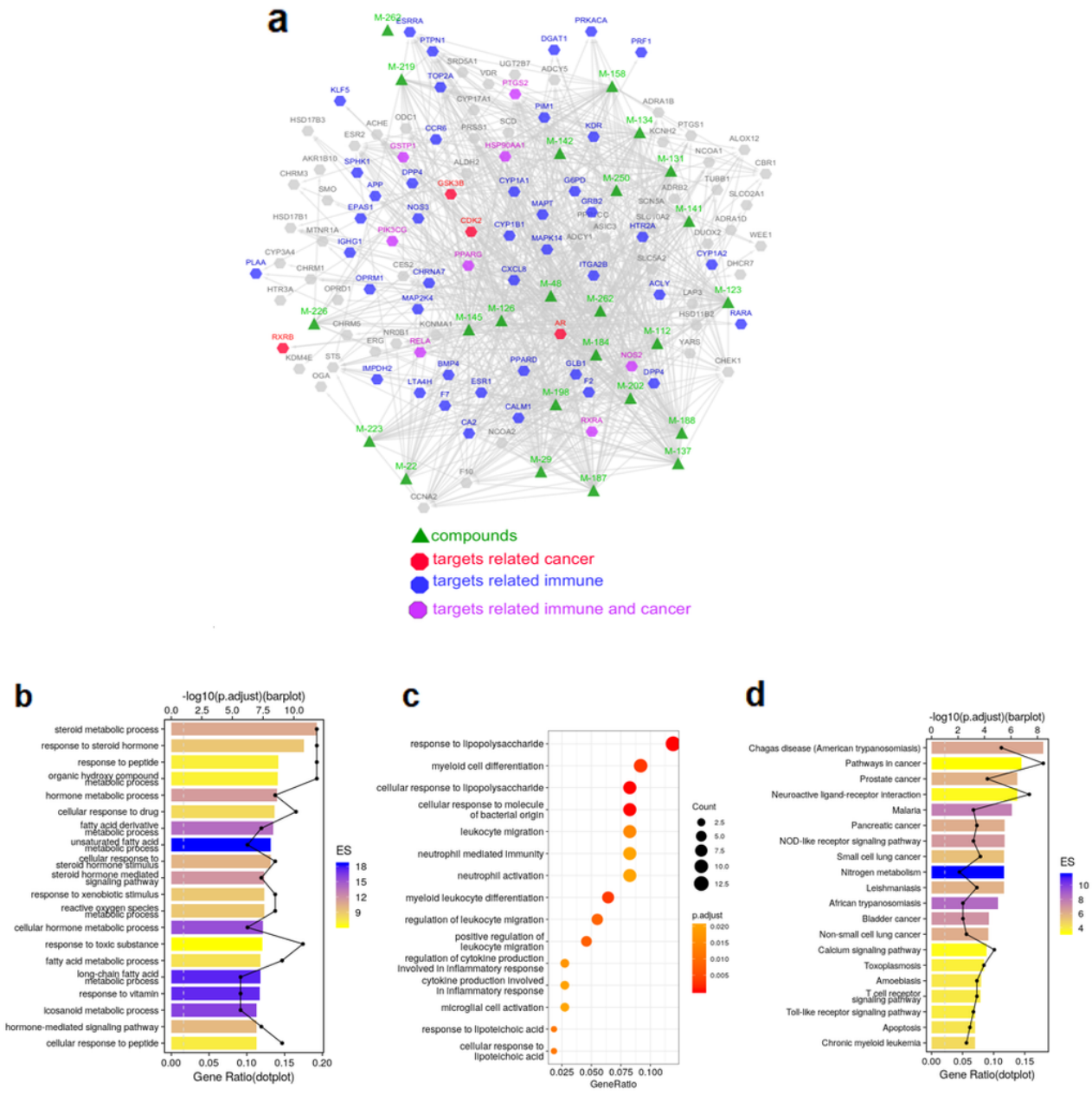

Figure 2

Systems pharmacology analysis of targets of licorice a Construction of compound-target network, the triangle represents compounds, the octagon represents targets, the edge represents connection between compounds and targets. b GO enrichment analysis of potential targets of licorice, the y-axis represents the enriched GO term, and the GeneRatio represents the number of targets located in this GO/the total number of targets located in the GO. c GO term associated with immune process were shown, and the size of the circle represents the count. d KEGG analysis of targets of licorice, the color represents the enrichment significance, the y-axis represents pathway, and the GeneRatio represents the number of targets located in this KEGG pathway/the total number of targets located in the KEGG pathways.

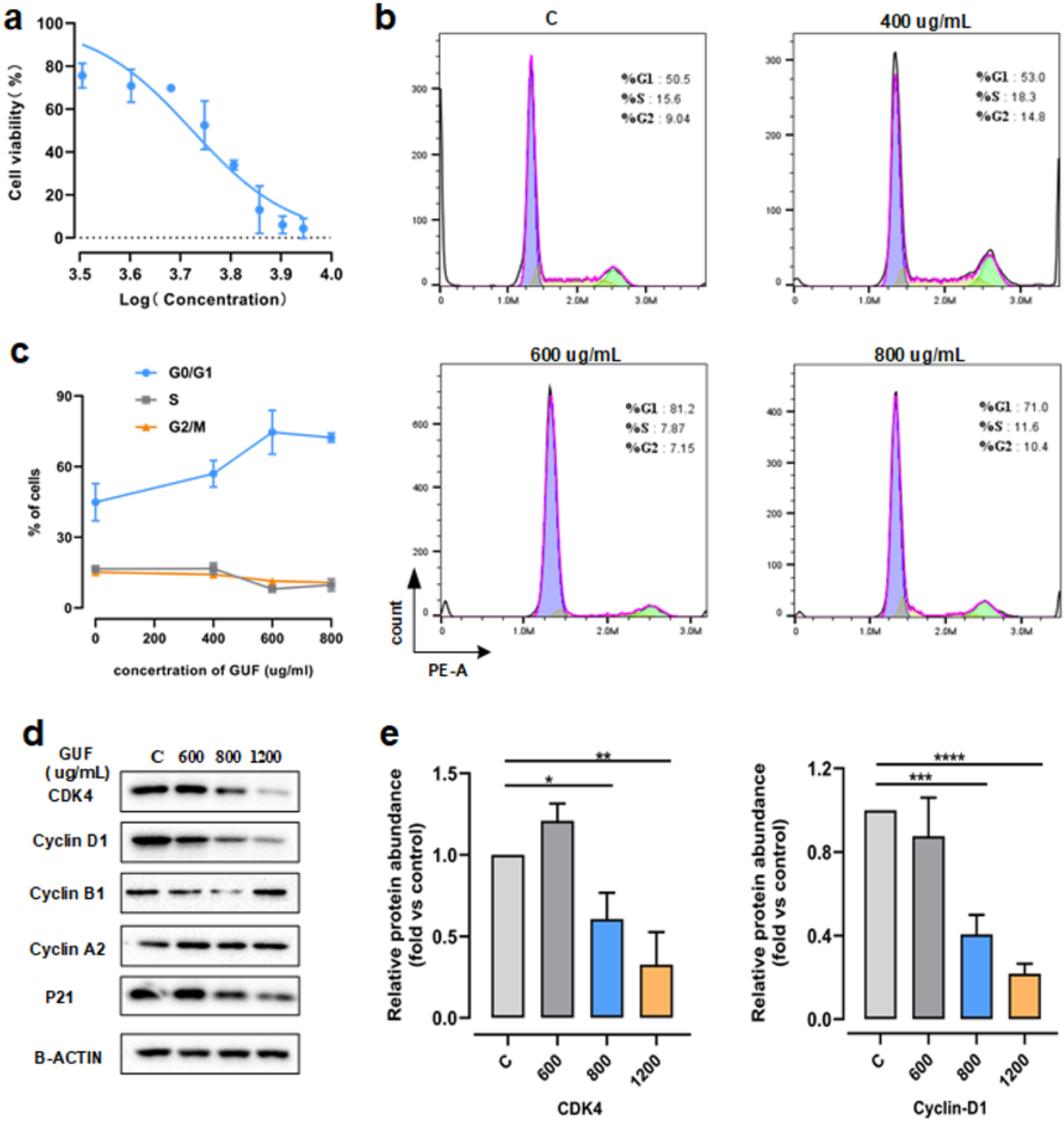

Figure 3

Licorice induce tumor cell G0/G1 phase arrest with the degradation of CDK4-Cyclin D1 complex. a H1975 cells were treated with different concentrations of licorice for 48 h, cell viability was determined using the CCK8 assay. (mean ± SE, n=5). b The cell-cycle profiles of H1975 cells that were incubated with 400、600、800 μg/ml GUF or vehicle control for 48 hours were shown by using fluorescence-activated cell sorting (FACS). c Percentages of H1975 cells in (b) at different cell cycle states. d The protein expression in

H1975 cells pretreated with 400、600、800 μg/ml GUF or vehicle control were measured by immunoblots, versus β-Actin as a loading control. e Relative protein abundance of CDK4 and Cyclin D1 of (d). (*p < 0.05, **p < 0.01, ***p < 0.001, ****p < 0.0001)

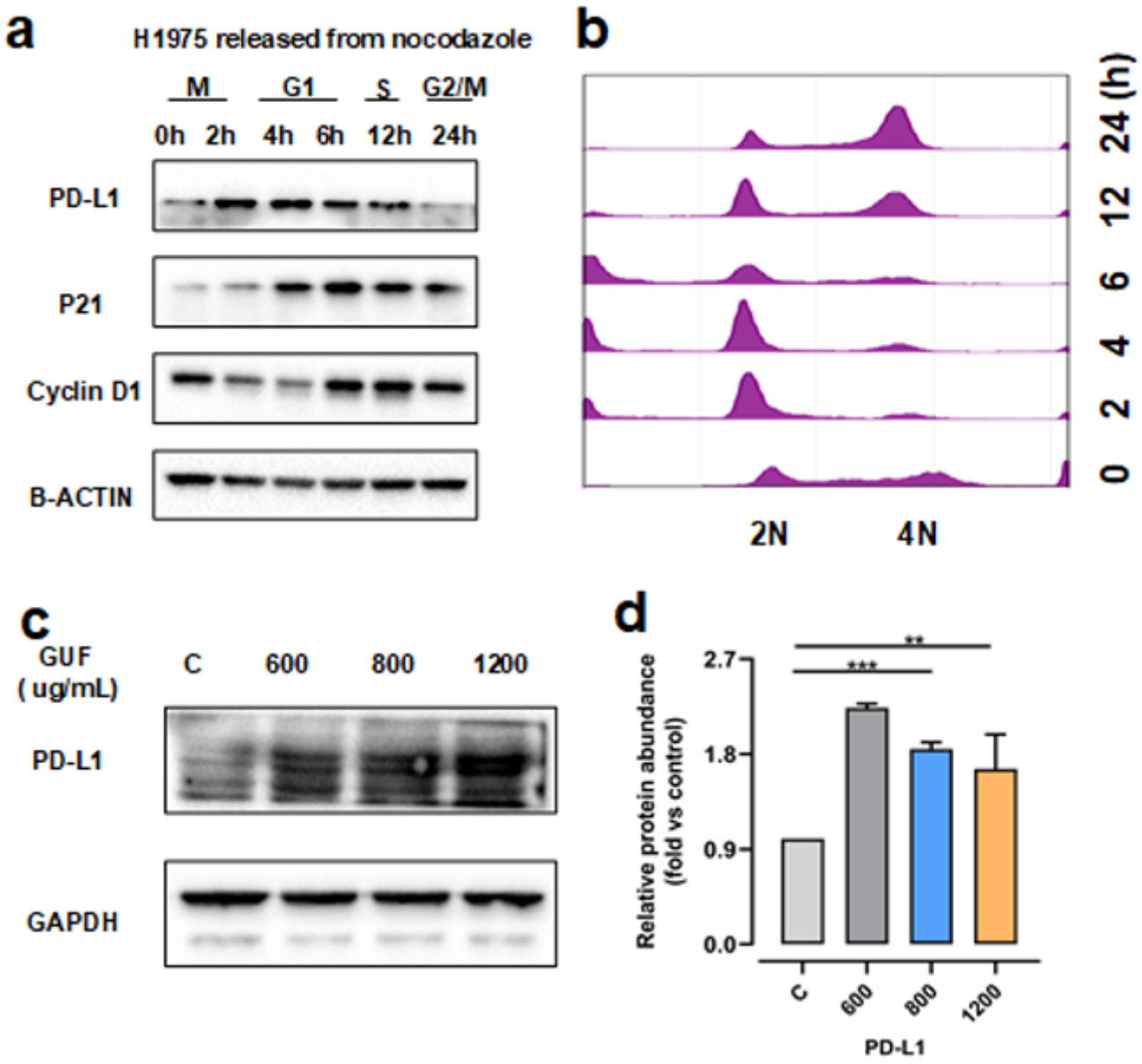

Figure 4

licorice induced increase of expression level of PD-L1 a Immunoblot (IB) results of whole cell lysates (WCL) derived from H1975 cells synchronized in M phase by nocodazole treatment prior to releasing back into the cell cycle for the indicated times. b The cell-cycle profiles in (a) were monitored by fluorescence-activated cell sorting (FACS). c The protein expression in H1975 cells pretreated with 400、600、800 μg/ml GUF or vehicle control, was measured by immunoblots, versus GAPDH as a loading control d Relative protein abundance of PD-L1 of (c). (*p < 0.05, **p < 0.01, ***p < 0.001, ****p < 0.0001)

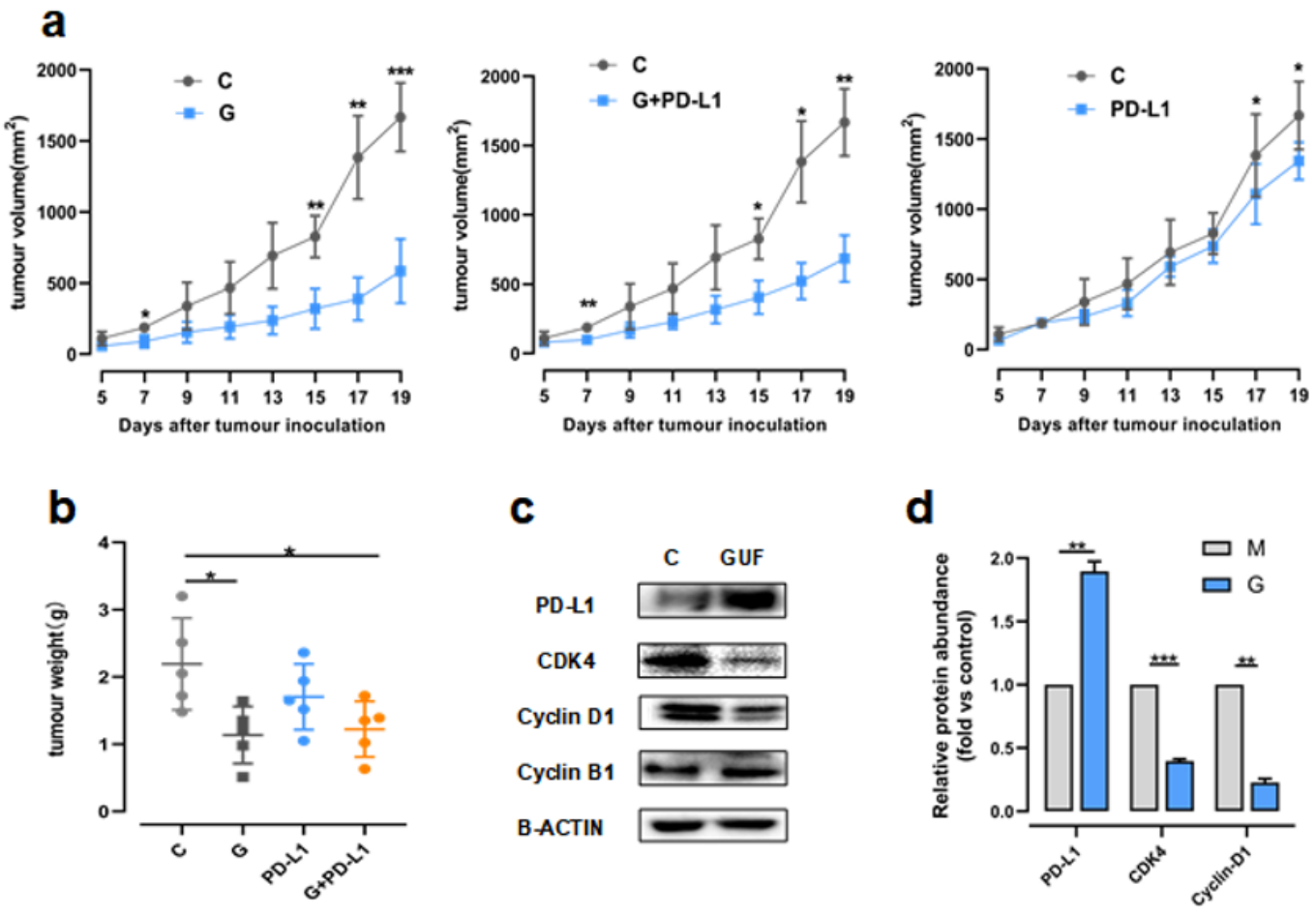

Figure 5

Licorice inhibit the growth of tumor volume depending on the Cyclin D1-CDK4-PD-L1 axis a C57 BL/6 mice were injected with 5*105 LLC cells. Beginning 24 hours later, 200 mg/kg GUF or vehicle or anti-PD-L1 (n = 5 per group) were administered once daily. The tumor growth curve is shown, with tumor sizes presented as mean ± SEM.*P < 0.05. b Primary tumor mass of mice is shown, presented as mean ± SEM. c Protein expression in tumors from GUF group and control group was measured by immunoblots, versus β-Actin as a loading control. d Relative protein abundance of PD-L1, CDK4, Cyclin D1, Cyclin B1 of (c), (*p < 0.05, **p < 0.01, ***p < 0.001.)

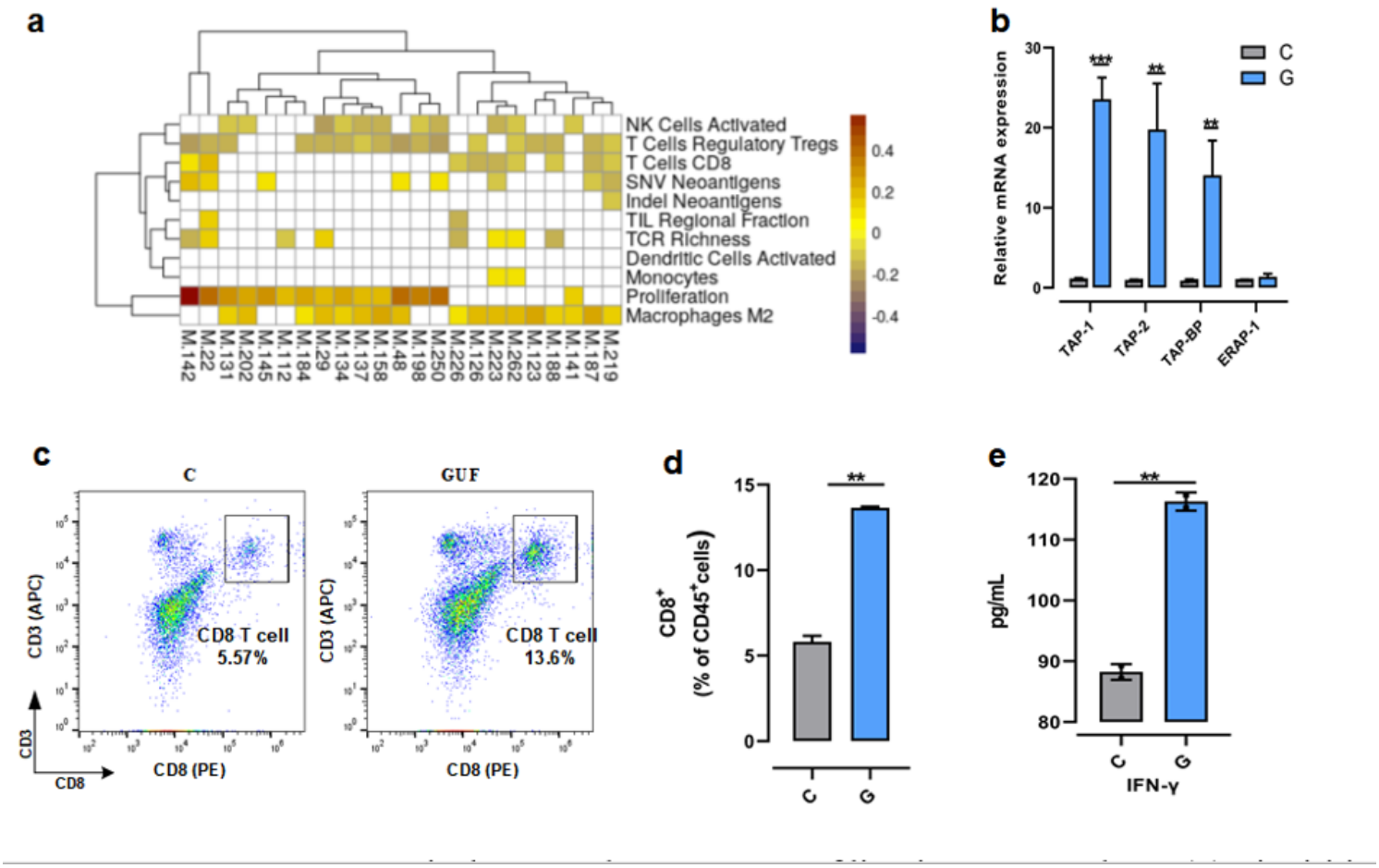

Figure 6

Licorice increased antigen presentation and infiltration of CD8+ T cell in vivo a Heatmap of Pearson's correlation coefficients (PCCs) between gene expression level of targets of licorice and immune phenotypes, the y-axis represents the compounds of licorice. b Relative Quantitative real-time PCR (q RT-PCR) analyses of relative mRNA levels of antigen presentation gene from licorice-treated tumors or vehicle. The experiments were repeated three times. Data was analyzed using ANOVA test. c Freshly isolated lymphocytes of tumor tissue samples from the GUF-treated group and control group were stained with anti-CD3, anti–CD45, and anti-CD8 antibodies and infiltration of CD8+ T cells examined by FACS. Representative flow-cytometry plots were shown. d Ratio of infiltration of CD8+ T cells in mice tumor samples from the GUF-treated group versus control group. e Bar graph of IFN-γ levels based on ELISA in mice tumor samples from the GUF-treated group and control group were shown. (**p < 0.01, ***p < 0.001.)

Supplementary Files

This is a list of supplementary files associated with this preprint. Click to download.

- Extendeddata.docx